Thermal Management of OLEDs Based on TADF Materials: Implication of Heat Upconversion to the Visible Light

Oleg Dimitriev

dimitr@isp.kiev.ua

V. Lashkaryov Institute of Semiconductor Physics https://orcid.org/0000-0002-6848-6401

Daria Kuznetsova

V. Lashkaryov Institute of Semiconductor Physics

Shih-Wei Huang

Fu-Chuan Fan

Petro Smertenko

Alexander Fedoryak

Dovydas Blazevicius

Gintare Krucaite

Saulius Grigalevicius

Chih-Hao Chang

Article

Keywords: thermally-activated delayed fluorescence, OLED, thermal management, activation energy, energy upconversion

Posted Date: July 3rd, 2025

DOI: https://doi.org/10.21203/rs.3.rs-6836729/v1

Additional Declarations: There is **NO** Competing Interest.

Thermal Management of OLEDs Based on TADF Materials: Implication of Heat Upconversion to the Visible Light

Daria Kuznetsova[#], Shih-Wei Huang[^], Fu-Chuan Fan[^], Petro Smertenko[#], Alexander Fedoryak[#], Dovydas Blazevicius[&], Gintare Krucaite[&], Saulius Grigalevicius[&], Chih-Hao Chang[^], Oleg Dimitriev[#],*

[#]V. Lashkaryov Institute of Semiconductor Physics NAS of Ukraine, pr. Nauki 41, Kyiv 03028, Ukraine

[&]Department of Polymer Chemistry and Technology, Kaunas University of Technology, Radvilenu plentas 19, Kaunas, LT50254, Lithuania

[^]Department of Electrical Engineering, Yuan Ze University, Taoyuan 32003, Taiwan

Abstract. High temperatures normally deteriorate the performance of light-emitting diodes, leading to excessive leakage currents, material degradation, and device failure. However, a thermal activation step is necessary for proper operation of OLEDs based on thermally-activated delayed fluorescence (TADF) compounds; therefore, heat might be exploited as a useful factor and as a side energy converted to the OLED emission. Here, we show that the performance of OLEDs based on two different TADF materials can be significantly improved by heating, where thermal management is extremely dependent on the applied biases. Device heating by ~30 K above room temperature causes enhancement of the OLED's electroluminescence by 5-6 times when operating near the turn-on voltage, while emission enhancement decreases at higher applied biases. At the same time, temperature dependencies of currents, current differential sensitivity, and activation energy for carrier injection behave differently, showing normal and abnormal regions, where currents increase and decrease with temperature, respectively. The discrepancy of temperature dependence of electroluminescence and current in the abnormal region provides increased external quantum efficiency and improved power efficiency of the device with increasing temperature. These findings suggest potential exploitation of TADF-based OLEDs in energy-saving applications and as energy upconverters pumping waste thermal energy to light emission.

Keywords: thermally-activated delayed fluorescence; OLED; thermal management; activation energy; energy upconversion

[*] Corresponding author, e-mail: dimitr@sp.kiev.ua

1. Introduction

Upconversion of thermal energy or low-energy infrared (IR) radiation to the visible range of the electromagnetic spectrum is a promising tool for providing a significant amount of additional energy that can be applied to assist in the operation of solar cells, photochemical extraction of hydrogen, energy storage, etc.[1,2,3] Such a tool, however, is far from a proper exploitation due to specific restrictions and drawbacks of conventional devices that collect and convert low-energy heat to electricity or other usable forms.[4] Among different operational principles of collection of thermal energy, such as THz and IR antennas, thermally-sensitive conformational changes of molecules, phase-change materials, photomechanical converters, etc.,[5,6,7,8] one-photon upconversion processes have deserved remarkable attention recently. A one-photon process of energy upconversion does not require a sensitizer or intensive excitation conditions and can employ thermal energy at environmental temperatures.[9] The one-photon energy upconversion can be particularly realized by using a thermally-activated delayed fluorescence (TADF), the process, where a triplet exciton converts to the singlet one through a reverse intersystem crossing (RISC) between excited triplet and singlet energy levels by absorption of heat, followed by the singlet radiative recombination (Fig. 1).

Recently, TADF has been widely used in organic light-emitting diodes (OLEDs) due to enhanced efficiency of conversion of injected charge carriers into light; however, exploiting such OLEDs as thermal energy upconverters can be considered a new perspective on their potential application. Therefore, relevant studies should be undertaken to clarify the details and efficiency of low-energy upconversion by such OLEDs.

Specifically, heat is one of the crucial parameters influencing the operation of light-emitting diodes, particularly those based on organic materials, i.e., OLEDs. A secondary heat can be produced because of the device functioning, i.e., currents yielding Joule heating, or direct heat can be delivered by external sources; in most cases, heat deteriorates the performance of light-emitting diodes, leading to device failure. On one hand, elevated temperatures cause the reduction in resistance, which leads to excessive leakage currents; on the other hand, organic molecules cannot normally withstand high temperatures as heat may accelerate the chemical reactions within these materials, resulting in material degradation.[10,11] As the reverse saturation current increases exponentially with temperature, the device becomes more prone to leakage, which affects its efficiency. The turn-on or threshold voltage also normally decreases in inorganic diodes with temperature as carrier concentration increases and the potential barrier for the p-n junction becomes reduced.

On the contrary, heat can stimulate the functioning of OLEDs based on TADF emitters, since this is necessary to facilitate the RISC between excited triplet and singlet levels, followed by the singlet radiative recombination. However, except for some rare works in this direction, no systematic studies of this issue have been performed so far.

In this work, we follow the operation of TADF-based OLEDs at different temperatures and applied biases to find how the combination of the above two factors can bring optimal conditions for more effective heat upconversion to energy of the visible light. We revealed a specific region of the applied biases close to the turn-on voltage, which yields significant enhancement (up to six times) of the emission upon increasing temperature from room temperature to 50 °C. The mechanism of such amazing enhancement is analyzed based on the behavior of the current and activation energy of the processes.

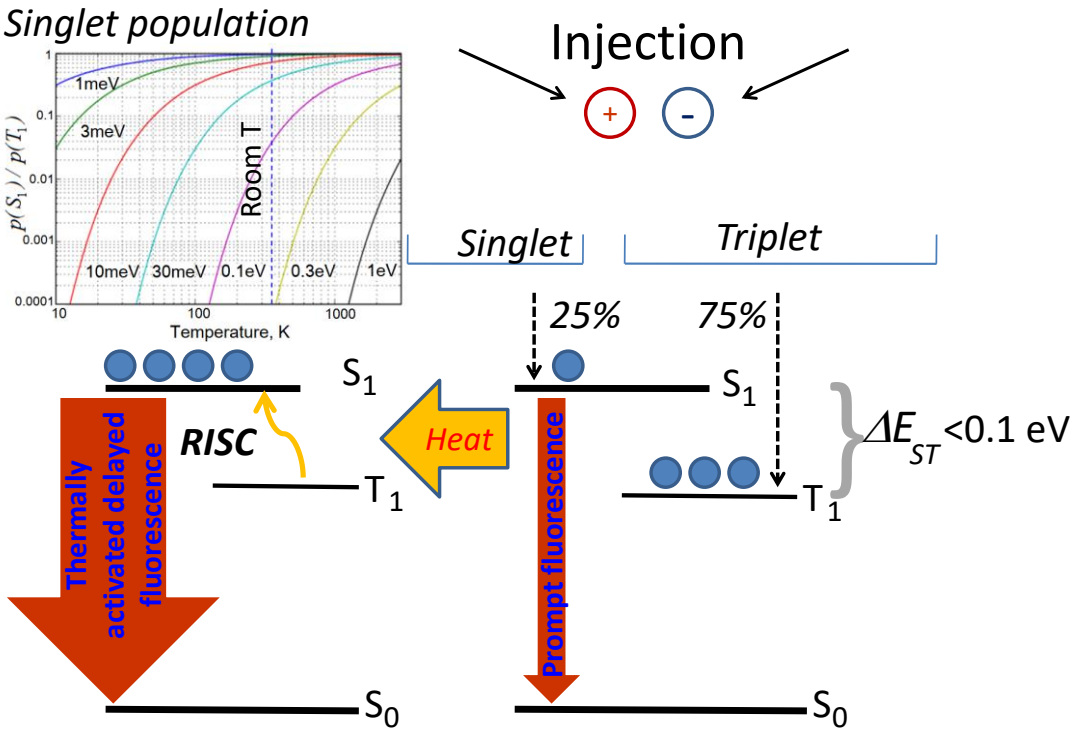

Fig. 1. Scheme of heat upconversion by TADF following injection of charge carriers in OLED. Population of the singlet level at different singlet-triplet energy gaps is shown as a function of temperature.

2. Methods

2.1. Materials and device preparation

To investigate the electroluminescent (EL) behavior of TADF OLEDs, we fabricated two devices utilizing yellow- and green-emitting TADF emitters. Specifically, we employed the commercially available yellow-emitting TADF emitter, *N*-(4-*tert*-butylphenyl)1,8-naphthalimide-9,9-dimethyl-9,10-dihydroacridine (**NAI-DMAC**), while the green-emitting TADF emitter, (4-(9*H*-carbazol-9-

yl)phenyl)(4-(3-(diphenylamino)-9*H*-carbazol-9-yl)phenyl)methanone (**EM2**), was developed in our previous research.[12,13] An optimal host material for such devices should provide efficient charge transport and balance, facilitate exothermic energy transfer to the guest molecules, and ensure effective exciton confinement. Given that exciplex formation results from the interaction between hole-transport and electron-transport materials, exciplex hosts generally exhibit superior charge transport capabilities, leading to reduced operating voltages. Based on our prior studies, we selected an exciplex host system composed of the donor material 4,4',4''-tris(carbazol-9-yl)triphenylamine (TCTA) and the acceptor material (1,3,5-triazine-2,4,6-triyl)tris(([1,10-biphenyl]-3-carbonitrile)) (CN-T2T) for both the yellow- and green-emitting devices, as this combination met all the requirements.[14] The electron transport layers (ETLs) in both devices were constructed using CN-T2T to ensure compatibility with the selected host system. Furthermore, to align the highest occupied molecular orbital (HOMO) energy levels and facilitate efficient hole injection, a double hole transport layer (HTL) configuration was implemented. This configuration combined 1,1-bis[(di-4-tolylamino)phenyl]cyclohexane (TAPC) with TCTA to establish a stepwise hole transport mechanism, thereby enabling smooth hole transfer from the HTL into the emitting layer (EML).[15] Additionally, utilizing the same material in the HTL (ETL) and EML helped eliminate energy barriers at the carrier transport layer/EML interfaces. This approach reduced charge accumulation at the interfaces, enhancing current density and improving device performance. TAPC was also employed as the host material for MoO_3 to form a p-type hole injection layer (HIL) for efficient hole injection.[16] This design facilitated band bending, enhancing hole injection from the anode into the organic layers. As a result, the optimized device architectures for the yellow- and green-emitting OLEDs, referred to further as Y and G devices, were as follows: ITO (120 nm)/TAPC doped with 20 wt.% MoO_3 (10 nm)/TAPC (35 nm)/TCTA (5 nm)/TCTA: CN-T2T (1:1) doped with 1 wt.% **NAI-DMAC** or 5 wt.% **EM2** (20 nm)/CN-T2T (50 nm)/LiF (1.2 nm)/Al (120 nm), where lithium fluoride (LiF) and aluminum served as the electron injection layer and cathode, respectively. The chemical structures of the employed materials and the schematic structures of the fabricated TADF OLEDs are presented in Figure 2.

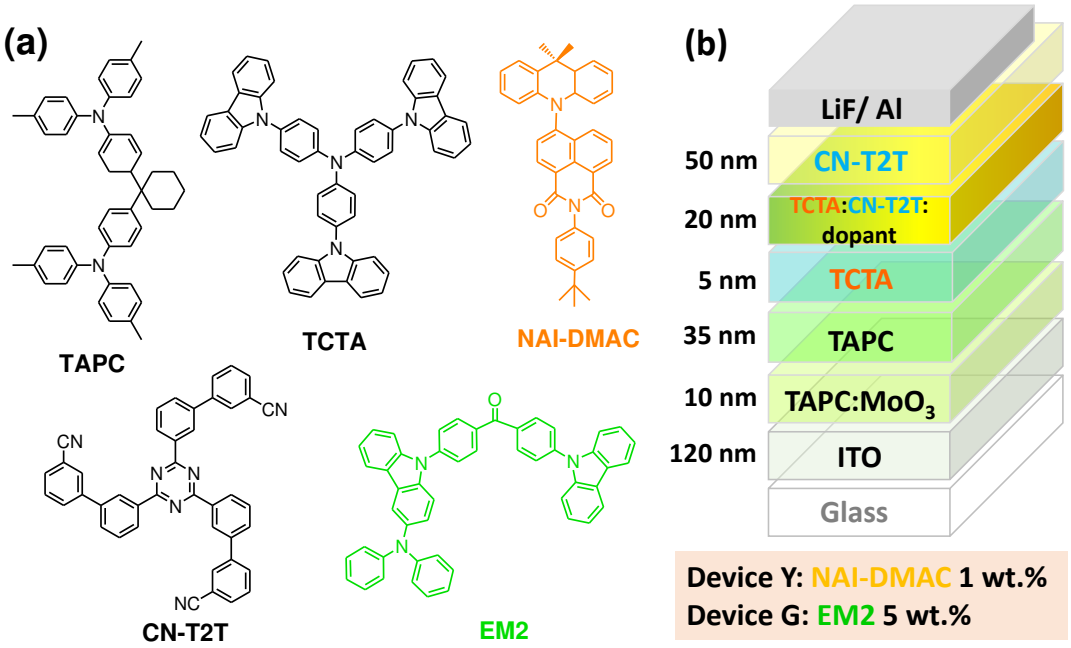

Fig. 2. (a) Structural drawings of the materials used; (b) schematic structures of the fabricated TADF OLEDs.

Before use, organic materials procured from Shine Materials Technology underwent temperature-gradient sublimation under high vacuum conditions. The ITO-coated glass substrates were cleaned through an ultrasonication process involving deionized water and organic solvents, followed by a 5-minute UV plasma pretreatment. The organic and metal layers were deposited via thermal evaporation in a vacuum chamber maintained at a < 10^{-6} Torr base pressure. Device fabrication was carried out in a single cycle without breaking the vacuum. The deposition rate of organic materials was maintained at approximately 0.1 nm/s. The shadow mask defines the circular lighting area with a diameter of 2.5 centimeters.

2.2. Measurements

UV-Vis and photoluminescence (PL) emission spectra of the samples were measured using an AvaSpec-2048 spectrometer through an optical 600 µm fiber. Emitted photons were registered by a CCD detector with thermoelectrical cooling to reduce noise contribution. NAI-DMAC was dissolved in toluene, and EM2 was dissolved in dichloromethane (DCM) as stock solutions with a concentration of 10^{-3} M, which were diluted to 10^{-5} M for optical investigations. Solutions were measured using a 10 mm quartz cuvette; pure solvent was used as a reference. The excitation was provided using a diode at 254 nm and diode solid-state lasers operating at 365 and 405 nm.

Basic characteristics of the devices were collected at ambient conditions and room temperature through measurement of current density-voltage-luminance dependencies by using two Keysight B2901A current source-measure units equipped with a calibrated silicon photodiode.

The electroluminescent spectra of the devices were recorded using an Ocean Optics spectrometer (Ocean Optics 2000).

For temperature measurements, OLED was placed in a home-made thermostat equipped with an oven. The sample was heated at a rate of about 1 degree per minute. Temperature was controlled with a thermocouple placed between the oven and the rear surface of the OLED and then corrected by separately measuring a temperature gradient between the rear and front surfaces of the device; the accuracy of the stated temperature values thus constitutes ±1 degree. EL emission spectra of the OLEDs were collected using an AvaSpec-2048 spectrometer. Temperature dependencies of current-voltage characteristics of OLEDs were measured by the SourceMeter Keithley-2410 instrument using the LabTracer software.

3. Results and Discussion

3.1. Basic characteristics of the OLEDs

Photophysical properties of TADF compounds used for manufacturing OLEDs were studied first in the form of solutions and thin films. PL spectra of diluted solutions showed the main PL bands located near 630 and 480 nm for NAI-DMAC and EM2, respectively, assigned to the charge-transfer (CT) emission [17], whereas the film spectra displayed CT emission bands at 580 nm for NAI-DMAC and at 550 nm for EM2 (Fig. 3a,b). The noticeable shift of the CT band and its narrowing in films compared to the solutions is associated with a high twisting disorder in the solution, and also different twisting conformations dominating in solutions and films, that is, a large number of different TADF conformers distributed in solution, while there are few in solid films.[18] EL emission spectra in OLEDs closely follow PL spectra of thin films, indicating the maximum at ~608 and 557 nm for the Y and G device, respectively (Fig. 3c).

Table 1. EL characteristics of the tested devices with different TADF emitters.

Device	Emitter	η_{ext} (%)/ η_L (cd/A)/ η_P (lm/W) [a]	η_{ext} (%)/η_L (cd/A)/ η_P (lm/W) [b]	V_{on} [c] (V)	λ_{max} [b] (nm)	CIE1931 coordinates (x, y) [d]	$L_{max.}$ (cd/m^2) [V]
Y	**NAI-DMAC**	11.0/ 19.6/ 26.8	9.9/ 17.7/ 20.8	2.2	608.5	(0.56, 0.43)	29,039 [9.0]
G	**EM2**	12.1/ 35.4/ 46.3	12.1/ 35.2/ 45.4	2.2	557.5	(0.43, 0.53)	60,155 [8.8]

[a.] Maximum efficiency; [b.] measured at 100 cd/m^2; [c.] turn-on voltage measured at 1 cd/m^2; [d.] measured at 1000 cd/m^2. [η_{ext}: external quantum efficiency; η_L: luminance efficiency; η_P: power efficiency; $L_{max.}$: maximum luminance].

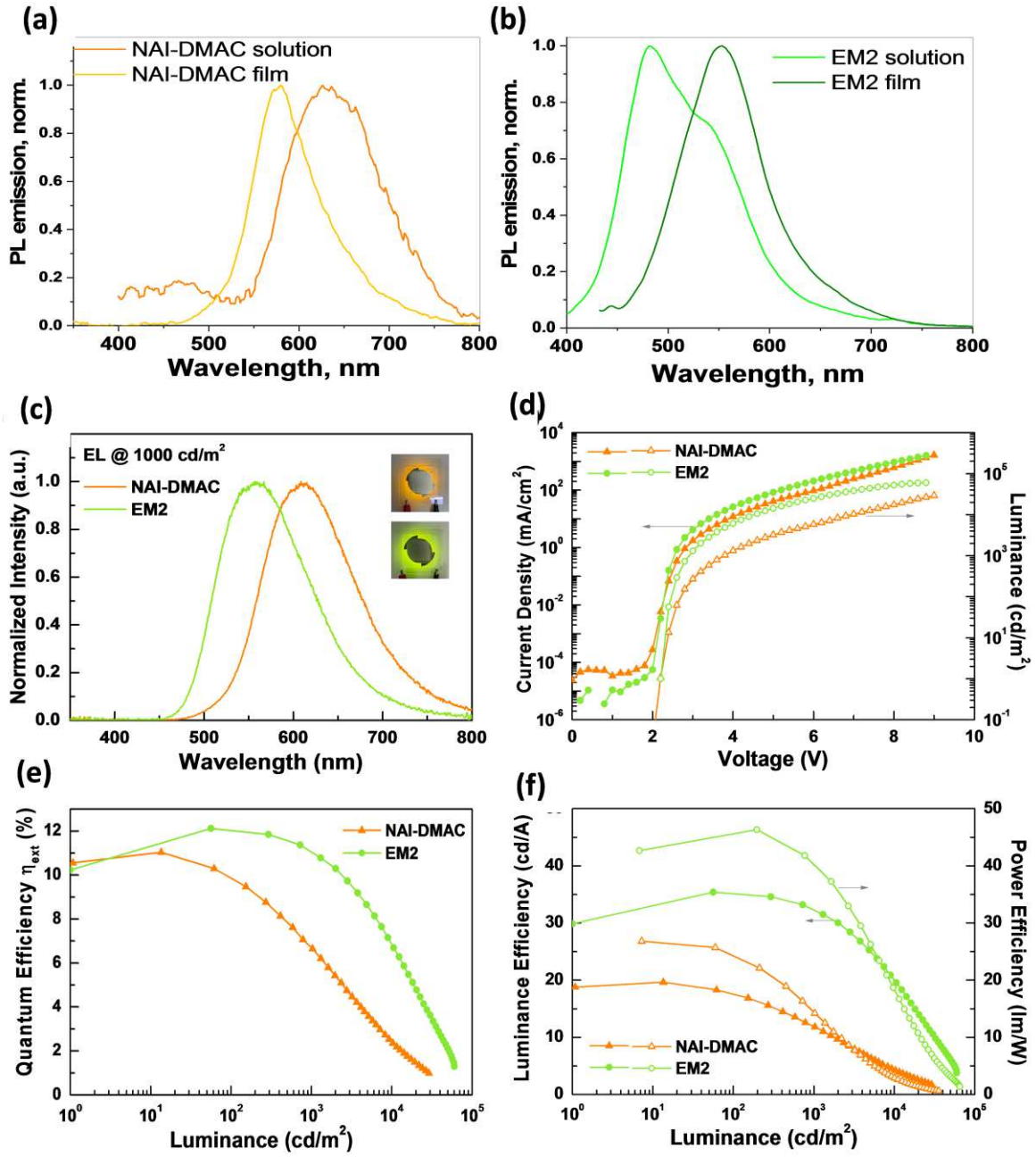

Fig. 3. PL emission spectra of dye solutions (10^{-5} M) and films of (a) NAI-DMAC and (b) EM2; (c) normalized EL spectra at a luminance of 1,000 cd/m^2 (insert shows visual emission of the Y and G devices); (d) current density-voltage-luminance (*J*-*V*-*L*) characteristics; (e) external quantum efficiency versus luminance; (f) luminance efficiency/power efficiency versus luminance for devices Y and G.

Figure 3(c-f) illustrates the electroluminescence (EL) characteristics of the fabricated TADF devices, with the corresponding numerical data summarized in Table 1. The normalized EL spectra of the devices, measured at a luminance of 1000 cd/m^2, are presented in Fig. 3(c). The pure emission from the TADF emitters confirms that the exciplex host enables efficient energy transfer from the host to the guest. The absence of emissions from the host or charge transport materials also verifies the excellent exciton confinement within the EML structure.[19] Both devices, Y and G, exhibited similar full width at half maximum (FWHM) values of approximately 119 nm, with peak emission wavelengths of 608.5 nm and 557.5 nm, respectively.

Figure 3(d) displays the current density-voltage-luminance (*J-V-L*) characteristics of the tested devices. Given that devices Y and G share nearly identical architectures except for the dopant, the charge transport properties of the TADF dopants primarily influence the current density. As shown, device G exhibited a higher current density than device Y, indicating the superior charge transport capability of **EM2**. For instance, at an applied voltage of 6 V, the current densities of devices Y and G were measured at 96.0 and 206.5 mA/cm^2, respectively. The luminance characteristics followed a similar trend, with maximum luminance values of 29,039 cd/m^2 for device Y and 60,155 cd/m^2 for device G. The significantly higher luminance observed in device G can be attributed to its higher current density and superior efficiency. Additionally, the increased candela value also results from the green emission spectrum aligning well with the human eye's higher spectral sensitivity.[20] Figures 3(e) and 3(f) present the efficiency curves of the devices. The maximum external quantum efficiencies (EQEs) of devices Y and G were recorded at 11.0% (19.6 cd/A and 26.8 lm/W) and 12.1% (35.4 cd/A and 46.3 lm/W), respectively. Furthermore, at a practical luminance level of 100 cd/m^2, the efficiency values were maintained at 9.9% for device Y and 12.1% for device G, corresponding to efficiency drops of 10.0% and 0%, respectively. These results suggest that devices utilizing exciplex host systems could maintain high efficiency due to an expanded exciton formation zone, which mitigates triplet-triplet annihilation and polaron quenching.[21] Therefore, these optimized devices are well-suited for use as illumination sheets in subsequent thermal experiments.

3.2. Thermal enhancement of the OLED emission

EL emission spectra of OLEDs measured at different applied voltages and temperatures varying from the room one to 40 ^{o}C, are shown in Fig. 4. The relative increase of the integral emission depends on the applied voltage and increases when the sample is heated up by ~ 22 degrees from room temperature by a factor up to 4 for the G device and by a factor of 5 for the Y device when the applied bias is close to the turn-on voltage. However, higher applied biases yield a smaller amplification factor that drops to about 1.3 at 6 V. Color maps (Fig. 4c,d) visually demonstrate the EL intensity amplification. The maps show that amplification increases with temperature under unchanged applied bias, with a steeper behavior when applied bias approaches the turn-on voltage. If the temperature is unchanged, amplification almost does

not change as a function of applied bias at room temperatures, whereas it changes more significantly at higher temperatures, showing enhancement upon decreasing applied bias.

Significant enhancement of the EL emission with temperature when the applied bias is close to the turn-on voltage makes such OLED an excellent upconverter of the heat energy to the visible light. For example, the temperature rise from 291 to 313 K yields an increase of the integral emission by a factor of 4 for the G device at 2.45 V and by 5 times for the Y device at 2.3 V. That is, the increase in the thermal energy by about 8% yields a gain in radiative energy by 300% and 400% for the G and Y devices, respectively. The mechanism of such fantastic energy upconversion efficiency can be understood based on the exponential dependence of the RISC process leading to population of the singlet energy level upon heating:

$$p(S_1) = p(T_1)\exp(-\frac{\Delta E_{ST}}{kT}) \qquad (1),$$

where $p(S_1)$ and $p(T_1)$ are the populations of singlet and triplet energy levels, and ΔE_{ST} is the S_1 to T_1 energy difference. According to Eq. (1), the increase in temperature of the emitter by 10% leads to an increase in singlet population by about one order of magnitude, followed by TADF emission (Fig. 1).

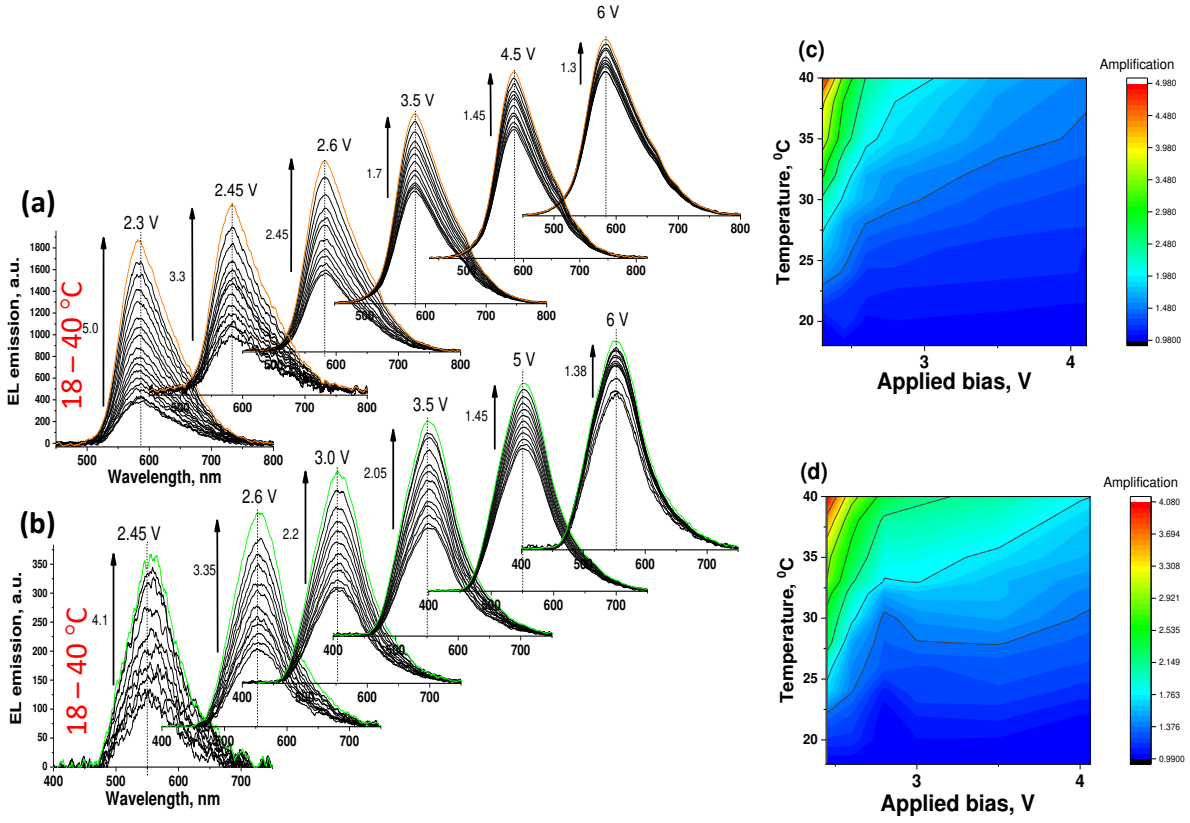

Fig. 4. (a,b) EL spectra and (c,d) 3D maps of the relative increase of EL emission as a function of the applied voltage and increasing temperature relative to that at room temperature: (a,c) Y device and (b,d) G device. The arrows in (a,b) quantify the EL enhancement with temperature.

3.3. Thermal enhancement of the OLED currents and EQE

In order to understand the mechanism of the above enhancement of the OLED emission with temperature, i.e., whether it occurs due to increasing OLED's currents associated either with the increased charge carrier mobility or concentrations, the temperature dependence of the currents at different applied biases has been studied.

It was found two regimes of current behavior as a function of temperature, which are dependent on the applied bias. First, in the range of applied biases near the turn-on voltage (i.e., near 2.2 V) extending to the isoconductive points at 2.3 and 2.75 V for the Y and G device, respectively (Fig.5), the current clearly decreases with temperature or has temperature regions with the decreasing current as a function of temperature. This regime will be referred to as abnormal. A second regime takes place at applied biases higher than the isoconductive points and corresponds to the normal behavior when current increases with temperature. The latter behavior is typical for disordered organic semiconductors, where higher temperatures improve charge carrier transport by adding the energy that facilitates overcoming the barriers created by energetic disorder.[22,23] This behavior also indicates that the transport here is hopping and needs thermal activation.

The abnormal regime of the current observed at low applied bias can be associated with the interplay between off-diagonal and diagonal disorder, which is influenced by temperature. When the former dominates the latter, the hopping transport of charges at low electric fields may follow the best percolation pathways, i.e., moving around the structural defects instead of colliding with them, whereas at higher applied fields the charge carrier moves with a stronger directionality and experiences a higher probability of collisions.[24] However, increasing temperature in the abnormal regime enhances scattering processes too, particularly due to the higher amplitude of vibrations, including those from defects, thus affecting percolation pathways, reducing mobility of charge carriers and resulting in decreased current, respectively. Thus, the interplay of temperature and applied electric field determines the complex transport behavior in the OLED structure near the turn-on voltage.

The transition region of applied biases near isoconductive points can be determined as that extending from the turn-on voltage of 2.2 V to 2.8 V for the Y device and from the turn-on voltage of 2.3 V to 3.75 V for the G device, which yields the most favorable conditions for current enhancement with temperature, that is, the ratio of current measured at increased temperature to current measured at room temperature (Fig. 6). The applied biases at 2.8 V and 3.75 V for the Y and G device, respectively, yield the maximal current amplification factor being 2.3 and 1.8 as measured at temperature of 51±1 ^{o}C in respect to room temperature, respectively (Fig. 6a,b). The current amplification factor decreases in the normal region with increasing applied bias, whereas it increases in the abnormal region, reaching a maximum, for all studied temperatures for the Y device and for temperatures above 40 ^{o}C for the G device (Fig. 6 a, b).

A deeper insight into the current behavior can be described by a differential technique, i.e., the analysis of current-voltage characteristics through calculation of the dimensionless sensitivity, *DS*:

$$DS(V) = \frac{d\log(I)}{d\log(V)} \quad (2).$$

The differential technique allows one to observe small deviations and is particularly useful for revealing the presence of traps,[25,26] where empty energy levels of the TADF molecules act as the trapping sites where the carriers are injected. A sharp peak in the behavior of *DS(V)* clearly marks a signature of traps [25] and is determined by interplay of different processes, such as (i) carrier injection to triplet and singlet levels of the emitter and exciton formation, (ii) radiative recombination of exciton, and (iii) exciton dissociation. The increasing region of *DS*>2 before peaking corresponds to dynamics of carrier injection and exciton recombination, where the former process exceeds the latter. Trap filling occurs via population mostly of triplet energy levels of the emitter, according to the spin statistics. This is related to the abnormal region of the *DS* behavior. The abnormal region starts at voltages below the turn-on one and extends to 2.8 V and 3.75 V for the Y and G devices, respectively. Here, heating promotes trapping of the injected carriers, since increasing temperature facilitates their hopping and collisions with traps, which is observed as smearing and shift of *DS* values to lower voltages (Fig. 6c,d). Such a behavior can be described by a Gaussian distribution of traps,

$$g_{ST} = \frac{N}{\sigma\sqrt{2\pi}}\exp(-\frac{1}{2}\frac{E_{ST}^2}{\sigma^2}) \quad (3),$$

where the variance σ increases with temperature. The variance relates to the dispersion of the triplet energy level and the singlet-triplet energy gap E_{ST}, respectively, due to increasing twisting disorder of the TADF molecules with temperature, where E_{ST} depends on molecular conformation. Thus, heating-induced twisting variation leads to variation in the energy gap E_{ST}, which overall facilitates RISC and therefore increases emission probability.

The isosensitive point in differential sensitivity behavior, i.e., the point where all *DS* curves cross and therefore are independent of temperature, is shown by the vertical dashed line (Fig. 6c,d). This point corresponds to equilibrium between trap filling, i.e., the exciton formation, and exciton recombination, followed by a decreasing region of *DS* where an excess of free carriers takes place, while the above equilibrium persists. As the amount of the free carriers becomes dominating, their behavior is described as temperature-induced hopping in a disordered semiconductor, where increasing temperature facilitates barrier overcoming and also trap release, and therefore leads to increasing current. This corresponds to the normal regime of the *DS* behavior. It is important to note that the isosensitive point in *DS* marks the maximal current enhancement (Fig. 6a,b).

Thus, the availability of the abnormal and normal regions of the *DS* behavior leads to the current enhancement, which is different from the EL emission enhancement at specific applied biases. While the amplification factor of the EL emission increases permanently upon decreasing bias, the amplification factor of the current increases in the normal region but then decreases in the abnormal region with decreasing bias (Fig. 6e,f). That means that the external quantum efficiency (EQE) of OLEDs increases in the abnormal region, too. We estimate that the relative increase of EQE for the Y device occurs up to a factor of 7.4 and up to 3.8 for the G device at a temperature of 51±1 ^{o}C.

The different enhancement behavior of the EL emission and currents can be explained by the gradual population of the triplet energy levels of the emitters when applied bias lies in the abnormal region, while the ratio of the singlet to triplet excitons remains the same, that is, 1:3, according to the spin statistics of the injected carriers. That means that while the concentration of singlet excitons is not saturated and singlet energy levels remain empty or partly populated, RISC can be realized by heat. In the normal region, where all triplet levels are completely populated, only the concentration of singlet excitons increases. More populated singlet levels then block RISC as each energy level can accept only two electrons according to the Pauli principle; therefore, enhancement of the emission due to heat becomes ineffective and leads to a smaller amplification factor with increasing applied bias. At the same time, increasing electric field is known to cause quenching of EL emission in OLEDs due to the field-induced dissociation of excitons and quenching of excited states due to the injected charge,[27,28,29] which can also contribute to the reduced enhancement of emission with temperature at high biases.

The increasing temperature was found to improve the power efficiency of the OLEDs too. For that, OLED emission at constant current in the normal regime was studied while changing the temperature. The constant current regime yielded practically unchanged integral EL emission at different temperatures, whereas the applied bias gradually decreased upon increasing temperature (Fig. 7). That means that the heat input to OLED is accompanied by decreasing the consumed power overall and that with increasing temperature less power consumption is needed to provide the same luminosity. It should be noted that the applied biases varied from 2.75 to 3.2 V for the Y device and from 3.6 to 4.2 V for the G device, which correspond to the normal regime of the current and *DS* behavior, where EL emission should increase with increasing current. Using the obtained data (Fig. 7c,d), we estimate that the power efficiency increases by 16% for the G device and by 13% for the Y device when heating from room temperature to 50 °C.

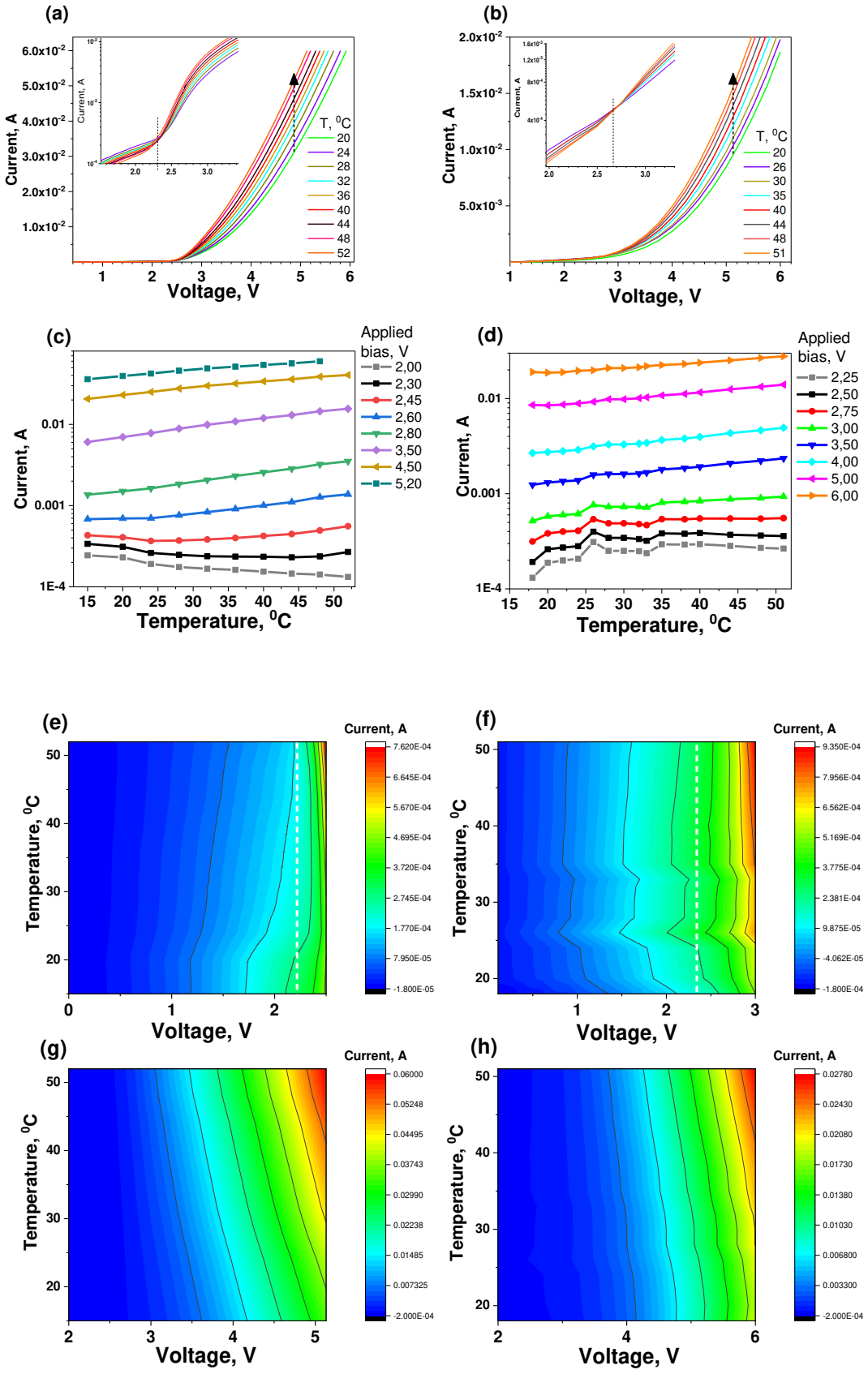

Fig. 5. (a, b) Current as a function of temperature at selected applied voltages (the temperature is indicated in the legend; the inserts show zoomed region near the turn-on voltage in a semi-

log scale, with isoconductive point indicated by dashed line); (c,d) current as a function of temperature at specific applied biases (shown in the legend); (e-f) 3D maps of current as a function of temperature and applied bias: (c,d) close to the turn-on voltage (marked by a vertical dashed line) and (e,f) in a broader voltage range for (a,c,e,g) Y device and (b,d,f,h) G device.

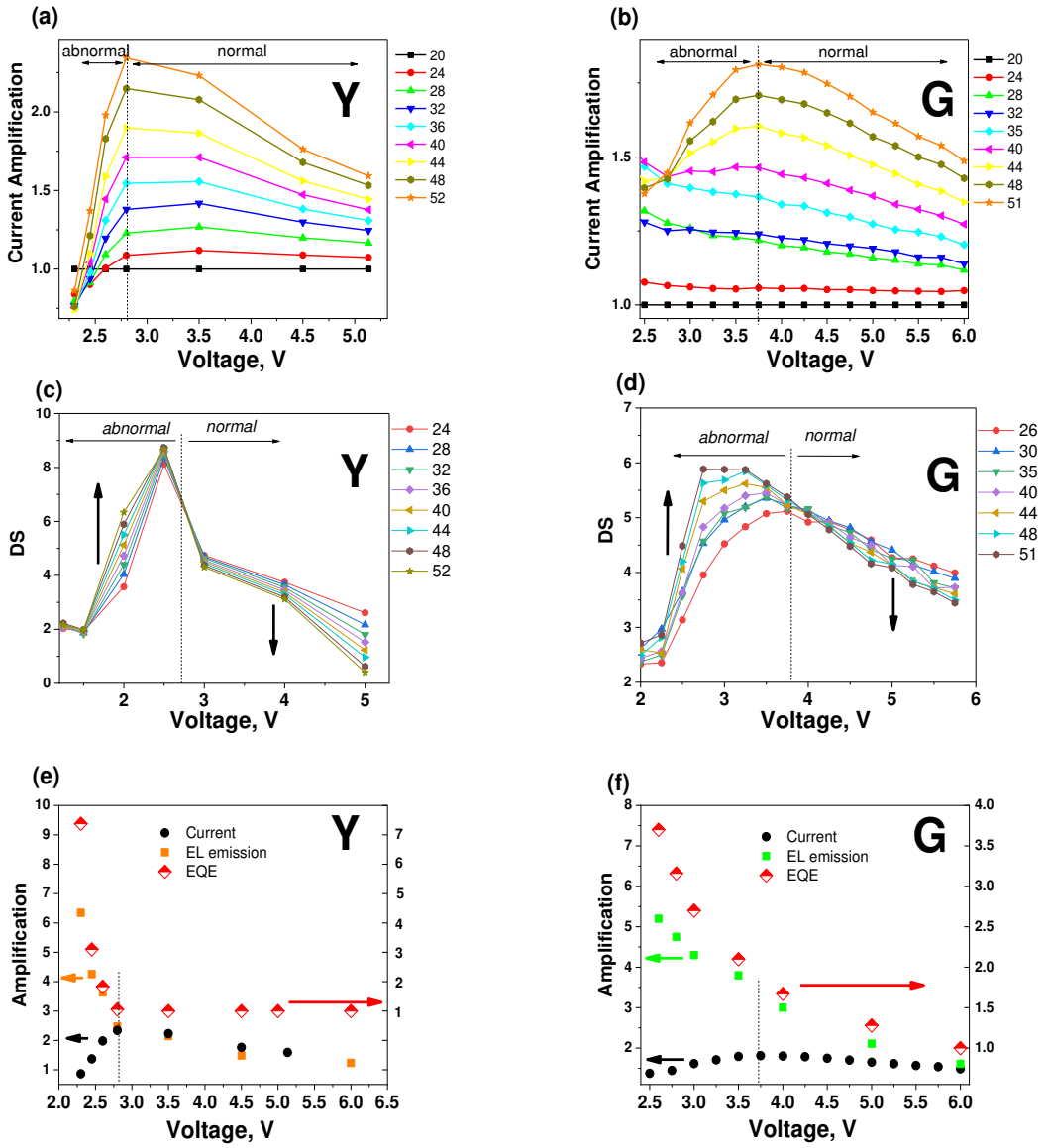

Fig. 6. (a,b) Amplification of the current at the indicated temperature (shown in the legend in °C) relatively to the current at room temperature as a function of the applied bias; (c,d) DS as a function of applied bias at the indicated temperature (shown in the legend in °C) and (c,d) comparison of amplification of the current (circles), EL intensity (squares), and EQE at 50 °C relatively to that at room temperature for (a,c) Y device and (b,d) G device. The vertical dashed lines in graphs mark the isosensitive point.

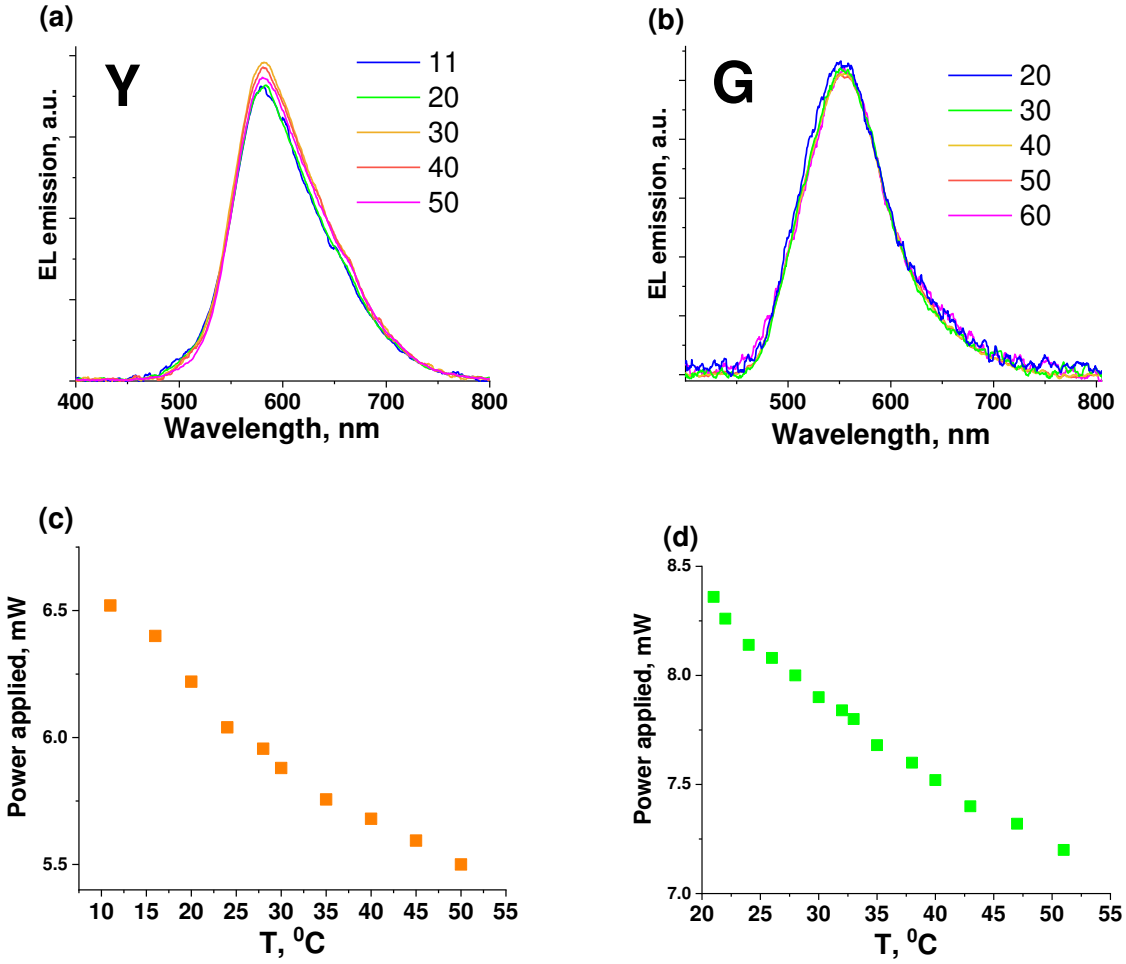

Fig. 7. (a,b) EL emission spectra and (c,d) power consumed by the OLEDs as a function of temperature under a constant current regime of 2 mA for (a,c) Y device and (b,d) G device. In (a,b) the temperature is indicated in the legend in °C.

3.4. Activation energy

Determining the activation energy for carrier injection and carrier transport allows one to better understand the mechanisms of the above carrier enhancement with increasing temperature as well. As discussed, the transport behavior in the samples is hopping and needs thermal activation. The higher the activation energy, the stronger the effect of temperature, i.e., the higher amplification factor for the current should be expected. Activation energy for charge transport can be determined from the Arrhenius plot of the temperature dependence of carrier conductivity or carrier mobility μ (which are both linearly related to current density),[22] although one should be aware of specific limitations of the analytical Arrhenius fit: [30]

$$\mu(T) = \mu_{\infty} \exp(-\frac{\Delta}{kT}) \quad (4),$$

where *k* is the Boltzmann constant, and Δ the activation energy, which can also be considered as a trapping energy in the multiple trapping and release (MTR) model,[31] where traps are due to the local structural disorder and are dispersed homogeneously.

Therefore, trapping by structural defects can be increased at higher applied fields when the charged carrier moves with a stronger directionality and experiences a higher probability of collisions with defects, as was discussed in the previous section. That is consistent with increasing activation energy at applied bias up to 2.8 V for the Y device and up to 3.8 V for the G device (Fig. 8). However, the activation energy then decreases at higher biases (Fig. 8); this can be explained by the fact that the most traps are filled in this region and therefore barriers for carrier hopping decrease. Also, the field dependence of the carrier mobility should be considered, which generally obeys a Poole-Frenkel behavior in the range of 10^4–10^6 V/cm [32,33]:

$$\mu(F) = \mu_0 \exp(\gamma\sqrt{F}) \quad (5),$$

where *F* is the electric field, and the negative γ determines decreasing values of mobility with applied bias.[34]

In the normal region, the calculated activation energies of carrier hopping lie in the range of 150-200 meV for the Y device and in the range of 100-150 meV for the G device, which falls in the same order of magnitude observed for other disordered organic semiconductors[35,36]

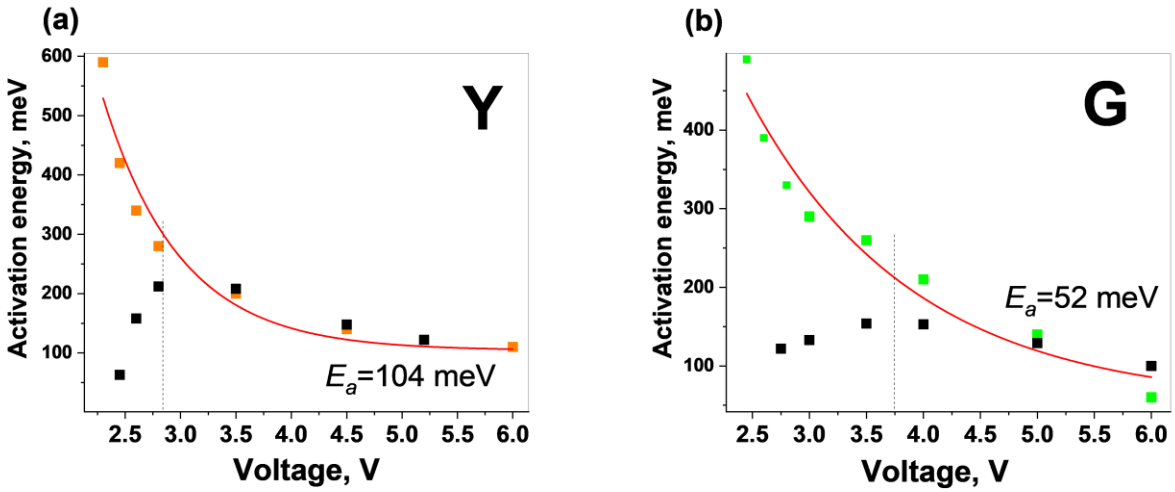

Fig. 8. Activation energy for EL ((a) yellow and (b) green symbols) and for carrier injection (black symbols) as a function of applied bias for (a) Y device and (b) G device. The vertical dashed line corresponds to the isosensitive point that separates normal and abnormal regions.

Activation energy for EL emission can also be extracted from the Arrhenius plot of emission intensity as a function of temperature (see Fig. 4):

$$I(\lambda) = \exp(-\frac{E_a}{kT}) \quad (6),$$

where $I(\lambda)$ is the integral intensity of the EL emission, E_a is the activation energy, and k is the Boltzmann constant.

It was found that the activation energy gradually changes with applied voltage, increasing by a factor of six for the Y device and almost by ten times for the G device when applied bias decreases from 6 V towards the turn-on voltage (Fig. 8). The dependence of activation energy on the applied bias can be fitted by the equation:

$$E_a(V) = E_{a0} + A\exp(-(V - V_0)/k) \quad (7),$$

where E_{a0} is the activation energy at $V \to \infty$, V is applied bias, V_0 is the turn-on voltage (taken as 2.25 and 2.38 V for the Y and G devices, respectively), A and k are constants.

Here, the activation energy E_{a0} corresponds to the singlet-triplet energy gap of the emitting molecules; it is equal to 104 meV for the Y device and 52 meV for the G device (Fig. 8), which agrees well with the singlet-triplet energy gap for NAI-DMAC (90 meV [17]) and EM2 (40 meV [13]) dyes determined elsewhere by spectral methods.

The abnormal increase of the activation energy with decreasing applied bias can be understood due to the fact that at low applied bias, the excitons are not massively formed yet, i.e., the exciton energy levels are poorly populated, in contrast to high applied biases where population of such levels is close to saturation. Formation of an exciton is a two-step process: first, injection of free carriers occurs to the transport energy levels, followed by binding of electron and hole to a quasi-particle called an exciton. However, in disordered semiconductors, stabilization of free electrons and holes may occur in the form of large polarons, which creates an energy barrier for the subsequent formation of excitons.[37,38] Therefore, thermal activation is needed to overcome this barrier and create excitons. To prevent the reverse process of exciton dissociation to polarons, the stabilization energy of the exciton, i.e., the binding energy, should be at least the same as that of the polaron barrier. Taking into account that an exciton binding energy in organic semiconductors is about one-quarter of the transport gap regardless of the materials,[39] we estimate the exciton binding energy to be about 0.6 eV for NAI-DMAC and about 0.5 eV for EM2, respectively. The estimated values agree well with activation energies for the Y and G devices near the turn-on voltages, respectively (Fig. 8). Thus, activation energy as a function of applied bias describes two processes: formation of excitons at low biases when their concentration is low, and triplet-singlet energy barrier at high biases where triplet energy levels are fully populated and triplet excitons have been completely formed.

Conclusions

In this work, the potential of heat upconversion to the visible light through thermal management of the TADF-based OLEDs was demonstrated. We showed that the performance of OLEDs based on two different TADF materials can be effectively tuned by temperature. In addition, applied bias plays an important role in controlling the temperature dependence of the OLED currents and emission significantly. Specific regions of the applied biases have been identified as the normal and abnormal ones. These regions are separated by isosensitive and isoconductive points for the *DS* and current behavior, respectively, where the former is important from the practical point of view, as it marks the maximal current enhancement and corresponds to the equilibrium between trap filling, i.e., the exciton formation, and exciton recombination. In the normal region, currents increase with temperature as expected for the disordered semiconductor, accompanied by the modest (~ 40-50%) enhancement of the OLED emission too. In the abnormal region, when applied biases are close to the turn-on voltage, the OLED emission becomes greatly sensitive to temperature, and the OLED's electroluminescence can be significantly enhanced by 5-6 times when heating up the device to ~50 °C. While EL emission increases, currents decrease with temperature in the abnormal region, providing enhancement of the external quantum efficiency and power efficiency of the devices by factors of 7.4 and 1.13 for the Y device and by 3.8 and 1.16 for the G device, respectively, upon heating from room temperature to ~ 50 °C.

However, exploiting or storing the devices at high temperatures may still be a challenging task due to potentially negative long-term impact of heat on device performance, which was not properly studied yet. By overcoming the related problems, the thermal management of the emission and related energy upconversion of TADF-based OLEDs promises potential application of this phenomenon for heat harvesting and energy-saving applications.

Acknowledgements

This work was supported by the Research Council of Lithuania (Grant No. S-LU-24-7), Ministry of Education and Science of Ukraine (project M/54-2024), and the National Science and Technology Council of Taiwan (NSTC 112-2923-E-155-002-MY4, NSTC 113-2221-E-155-014-MY3, and NSTC 114-2923-E-155-001-MY3). The authors are grateful to Dr. D. Grynko, Dr. V. Romanyuk, and Mrs. A. Kykot for technical assistance in experimental work.

Author contributions: CRediT

S.W.H., F.C.F., D.B., G.K., and A.F.: Resources and Data curation; D.K. and P.S.: Investigation and Formal analysis; S. G and C.H.C.: Project administration, Supervision and Writing – review and editing; O.D.: Conceptualization, Investigation, Writing – original draft, and Project administration.

Conflict of Interest

The authors declare no conflict of interest.

Data Availability Statement

The data that support the findings of this study are available from the corresponding author upon reasonable request.

References

[1] Shang, Y., Hao, S., Yang, C., & Chen, G. (2015). Enhancing solar cell efficiency using photon upconversion materials. *Nanomaterials*, *5*(4), 1782-1809.

[2] Wang, Z., Roberts, R. R., Naterer, G. F., & Gabriel, K. S. (2012). Comparison of thermochemical, electrolytic, photoelectrolytic and photochemical solar-to-hydrogen production technologies. *International journal of hydrogen energy*, *37*(21), 16287-16301.

[3] Dimitriev, O., Yoshida, T., & Sun, H. (2020). Principles of solar energy storage. *Energy Storage*, *2*(1), e96.

[4] Gamel, M. M. A., Lee, H. J., Rashid, W. E. S. W. A., Ker, P. J., Yau, L. K., Hannan, M. A., & Jamaludin, M. Z. (2021). A review on thermophotovoltaic cell and its applications in energy conversion: issues and recommendations. *Materials*, *14*(17), 4944.

[5] Mescia, L., & Massaro, A. (2014). New Trends in Energy Harvesting from Earth Long-Wave Infrared Emission. *Advances in Materials Science and Engineering*, *2014*(1), 252879.

[6] Kashyap, V., Sakunkaewkasem, S., Jafari, P., Nazari, M., Eslami, B., Nazifi, S., ... & Ghasemi, H. (2019). Full spectrum solar thermal energy harvesting and storage by a molecular and phase-change hybrid material. *Joule*, *3*(12), 3100-3111.

[7] Dimitriev, O. P. (2019). Harvesting of the infrared energy: Direct collection, up-conversion, and storage. *Semiconductor physics, quantum electronics & optoelectronics*, *22*(4).

[8] Dimitriev, O. P. (2023). Thermomechanical energy converters for harvesting thermal energy: A Review. *J. Renew. Mater*, *11*(4).

[9] Ma, L., Slattery, O., & Tang, X. (2012). Single photon frequency up-conversion and its applications. *Physics reports*, *521*(2), 69-94.

[10] de Moraes, I. R., Scholz, S., Hermenau, M., Tietze, M. L., Schwab, T., Hofmann, S., ... & Leo, K. (2015). Impact of temperature on the efficiency of organic light emitting diodes. *Organic electronics*, *26*, 158-163.

[11] Tyagi, P., Srivastava, R., Giri, L. I., Tuli, S., & Lee, C. (2016). Degradation of organic light emitting diode: Heat related issues and solutions. *Synthetic Metals*, *216*, 40-50.

[12] Zeng, W., Lai, H. Y., Lee, W. K., Jiao, M., Shiu, Y. J., Zhong, C., ... & Yang, C. (2018). Achieving nearly 30% external quantum efficiency for orange–red organic light emitting diodes by employing thermally activated delayed fluorescence emitters composed of 1, 8-naphthalimide-acridine hybrids. *Advanced Materials*, *30*(5), 1704961.

[13] Krucaite, G., Beresneviciute, R., Tavgeniene, D., Grigalevicius, S., Chen, Y. T., Chen, Y. H., & Chang, C. H. (2024). New bipolar derivatives with diphenylsulfone or dibenzophenone as TADF based emitters for OLEDs. *Organic Electronics*, *125*, 106981.

[14] Chen, W. L., Chen, S. Y., Huang, D. C., Luo, D., Chen, H. W., Wang, C. Y., & Chang, C. H. (2021). A method to realize efficient deep-red phosphorescent OLEDs with a broad spectral profile and low operating voltages. *Materials*, *14*(19), 5723.

[15] Gnanasekaran, P., Chen, Y. T., Tseng, Y. T., Su, K. Y., Lin, Y. T., Yiu, T. C., ... & Chang, Y. J. (2024). Perceiving the influence of phenyl-carbazole isomers on sulfone/thioxanthone-based D–A–D hosts: realizing efficient red-phosphorescent OLEDs. *Journal of Materials Chemistry C*, *12*(6), 2203-2215.

[16] Beresneviciute, R., Tavgeniene, D., Blazevicius, D., Chen, K. W., Chen, Y. H., Grigalevicius, S., & Chang, C. H. (2024). 9-(9-Alkylcarbazol-3-yl)-3-(methoxypyridin-3-yl) carbazoles as host materials for very efficient OLEDs. *Optical Materials*, *157*, 116273.

[17] Zeng, W., Lai, H. Y., Lee, W. K., Jiao, M., Shiu, Y. J., Zhong, C., Gong, S., Zhou, T., Xie, G., Sarma, M., Wong, K.T., Wu,C.-C., Yang, C. (2018). Achieving nearly 30% external quantum efficiency for orange–red organic light emitting diodes by employing thermally activated delayed fluorescence emitters composed of 1, 8-naphthalimide-acridine hybrids. *Advanced Materials*, *30*(5), 1704961.

[18] Tavgeniene, D., Krucaite, G., Blazevicius, D., Grigalevicius, S., Bogoslovska, A., Ali, A., ... & Dimitriev, O. (2025). Ethyl cellulose as a host material for thermally-activated delayed fluorescence emitters. *Optical Materials*, 117097.

[19] Chuang, T. H., Su, K. Y., Yang, Y. R., Chen, Y. T., Hsu, C. Y., He, Z. R., ... & Chang, C. H. (2025). Quinoxaline-based host materials for organic light-emitting diodes. *Optical Materials*, *159*, 116513.

[20] Jouaiti, A., Huang, D. C., Giuso, V., Cebrián, C., Mercandelli, P., Wang, K. H., ... & Mauro, M. (2023). True-to sky-blue emitters bearing the thiazolo [5, 4-d] thiazole electron acceptor for single and tandem organic light-emitting diodes. *ACS Applied Electronic Materials*, *5*(5), 2781-2792.

[21] Al Amin, N. R., Ho, C. Y., Huang, D. C., Chang, R. M., Cheng, Y. H., & Chang, C. H. (2025). Interfacial modification in multilayered charge generation layer structure for highly efficient charge generation in tandem OLEDs. *Chemical Engineering Journal*, *505*, 159509.

[22] Coropceanu, V., Cornil, J., da Silva Filho, D. A., Olivier, Y., Silbey, R., & Brédas, J. L. (2007). Charge transport in organic semiconductors. *Chemical reviews*, *107*(4), 926-952.

[23] Karl, N. (2003). Charge carrier transport in organic semiconductors. *Synth. Met.*, *133*, 649-657.

[24] Bässler, H. (1993). Charge transport in disordered organic photoconductors. A Monte Carlo simulation study. *Physica Status Solidi B (Basic Research);(Germany)*, *175*(1).

[25] Rizvi, S. M. H., Mantri, P., & Mazhari, B. (2014). Traps signature in steady state current-voltage characteristics of organic diode. *J. Appl. Phys.*, *115*(24).

[26] Rizvi, S. M. H., & Mazhari, B. (2018). Investigation of traps in thin-film organic semiconductors using differential analysis of steady-state current–voltage characteristics. *IEEE Transactions on Electron Devices*, *65*(8), 3430-3437.

[27] Rothe, C., King, S. M., & Monkman, A. P. (2005). Electric-field-induced singlet and triplet exciton quenching in films of the conjugated polymer polyspirobifluorene. *Physical Review B—Condensed Matter and Materials Physics*, *72*(8), 085220.

[28] Virgili, D., Cocchi, M., Fattori, V., Kalinowski, J., & Stampor, W. (2006). Large electric field effects on photoluminescence of organic Eu3+ complex-based electroluminescent emitters. *Applied physics letters*, *88*(5).

[29] Kalinowski, J., Mężyk, J., Meinardi, F., Tubino, R., Cocchi, M., & Virgili, D. (2008). Exciton quenching in emitter blends for organic light emitting devices probed by electric field–dependent time-resolved luminescence. *The Journal of chemical physics*, *128*(12).

[30] Züfle, S., Altazin, S., Hofmann, A., Jäger, L., Neukom, M. T., Brütting, W., & Ruhstaller, B. (2017). Determination of charge transport activation energy and injection barrier in organic semiconductor devices. *Journal of Applied Physics*, *122*(11).

[31] Horowitz, G. (1998). Organic field-effect transistors. *Advanced materials*, *10*(5), 365-377.

[32] Pai, D. M. (1970). Transient photoconductivity in poly (N-vinylcarbazole). *The Journal of Chemical Physics*, *52*(5), 2285-2291.

[33] Mozer, A. J., Denk, P., Scharber, M. C., Neugebauer, H., Sariciftci, N. S., Wagner, P., ... & Vanderzande, D. (2004). Novel regiospecific MDMO− PPV copolymer with improved charge transport for bulk heterojunction solar cells. *The Journal of Physical Chemistry B*, *108*(17), 5235-5242.

[34] Mozer, A. J., & Sariciftci, N. S. (2004). Negative electric field dependence of charge carrier drift mobility in conjugated, semiconducting polymers. *Chemical physics letters*, *389*(4-6), 438-442.

[35] Goh, C., Kline, R. J., McGehee, M. D., Kadnikova, E. N., & Fréchet, J. M. (2005). Molecular-weight-dependent mobilities in regioregular poly (3-hexyl-thiophene) diodes. *Applied Physics Letters*, *86*(12).

[36] Schwarze, M., Gaul, C., Scholz, R., Bussolotti, F., Hofacker, A., Schellhammer, K. S., ... & Leo, K. (2019). Molecular parameters responsible for thermally activated transport in doped organic semiconductors. *Nature materials*, *18*(3), 242-248.

[37] Simbula, A., Pau, R., Wang, Q., Liu, F., Sarritzu, V., Lai, S., ... & Bongiovanni, G. (2021). Polaron plasma in equilibrium with bright excitons in 2D and 3D hybrid perovskites. *Advanced Optical Materials*, *9*(16), 2100295.

[38] Motti, S. G., Kober-Czerny, M., Righetto, M., Holzhey, P., Smith, J., Kraus, H., ... & Herz, L. M. (2023). Exciton formation dynamics and band-like free charge-carrier transport in 2D metal halide perovskite semiconductors. *Advanced Functional Materials*, *33*(32), 2300363.

[39] Sugie, A., Nakano, K., Tajima, K., Osaka, I., & Yoshida, H. (2023). Dependence of exciton binding energy on bandgap of organic semiconductors. *The Journal of Physical Chemistry Letters*, *14*(50), 11412-11420.